Journal of Catalysis 266 (2009) 169–181

Contents lists available at ScienceDirect

Journal of Catalysis

journal homepage: www.elsevier.com/locate/jcat

Transport and sorption studies in beta and USY zeolites via temporal analysis of products (TAP)

Subramanya V. Nayak, Mehmet Morali, Palghat A. Ramachandran, Milorad P. Dudukovic *

Chemical Reaction Engineering Laboratory (CREL), Department of Energy, Environmental and Chemical Engineering, Washington University in St. Louis (WUSTL), MO 63130, USA

ARTICLE INFO

Article history:
Received 5 February 2009
Revised 11 May 2009
Accepted 9 June 2009
Available online 29 July 2009

Keywords:
Temporal analysis of products (TAPs)
Beta
USY
Zeolites
Intra-particle diffusion
Adsorption–desorption
Knudsen diffusion
Isobutane and *n*-butane

ABSTRACT

Single pulse TAP experiments were chosen for obtaining estimates of intra-particle diffusion coefficients and better insight into adsorption–desorption dynamics and equilibria for isobutane and *n*-butane in commercially available beta and USY zeolite. This technique provides a unique way of directly estimating transport and sorption processes at extremely low surface coverage ($\theta_i \to 0$), in the absence of an inert carrier stream, with no external mass transfer resistance, and with a negligible thermal effect. The use of a thin zone TAP reactor configuration enables the use of small zeolite particles without causing high bed resistance. A theoretical model that considers transport and adsorption–desorption phenomena in the inter-particle and intra-particle space is developed and numerically solved. Numerical experiments demonstrate the ability of the model to represent the actual experimental response curves. It is shown that reliable values of intra-particle diffusivity and adsorption–desorption constants can be obtained from the TAP single pulse experiments when the three dimensionless constants of the model τ_{p_i} (the ratio of characteristic diffusion time in the micro-reactor to characteristic diffusion time in zeolite pore), K_{eq_i} (the ratio of characteristic desorption time to characteristic adsorption time), and $k^*_{d_i}$ (the ratio of characteristic diffusion time in the micro-reactor to characteristic desorption time) fall within a prescribed range.

1. Introduction

Large pore beta and ultra-stable Y (USY) zeolites (pore range from 0.56 to 0.72 nm) have been extensively studied for their catalytic activity. Illustrative applications include alkylation of light hydrocarbons [1–4] catalytic cracking of heavy hydrocarbons [5–7], and isomerization of straight chain paraffins [8–11]. An improved understanding of the intra-particle diffusion and adsorption–desorption of various species in these zeolites is required for optimizing these catalysts, operating conditions, and regeneration protocols. However, there are only a few studies in the literature on beta and USY zeolites that report these intra-particle properties for hydrocarbons of interest [12–24]. Commercially, these zeolites are available in the form of self-aggregates with an average particle size of 5 μm and an average crystal size of 0.5 μm. These small crystals make it difficult to obtain reliable estimates of the intra-particle diffusivity and adsorption–desorption constants by conventional tracer techniques [25].

Theoretical predictions of transport coefficients and adsorption isotherms in these zeolites, while significantly advancing in the last decades [26–28] have not yet been able to yield results that can be accepted without experimental confirmation. For this reason many different experimental techniques have been tested for determination of the above-mentioned parameters but none has been universally adopted [13,14,18,19,21,25,29–33]. These studies can roughly be divided into two categories: macroscopic and microscopic. Most macroscopic experimental systems [13,14,18,19,25,29,32,33] introduce a concentration or pressure change of the probe molecules into a carrier stream continuously flowing over zeolites particles. The real time response of the probe molecules to such a perturbation is recorded at the exit. An appropriate theoretical model is used to represent the exit response and to estimate the desired parameters. Due to the presence of the carrier stream and external mass transfer resistance in most macroscopic experimental systems only a crude estimate of intra-particle diffusivity in small zeolite particles is possible [19,25]. Moreover, the high concentration of probe molecules in these experiments can induce a thermal effect due to sorption. This effect is more pronounced in the case of small zeolite particles [19,34] further decreasing the reliability of the estimated intra-particle diffusivity and adsorption–desorption constants. In microscopic experimental systems [30,31] the intra-particle diffusivity is directly calculated from the observed mean square displacement of the probe molecule. However, these techniques require the diffusing molecules to spend quite a long time in the intra-particle space,

* Corresponding author. Address: Department of Energy, Environmental and Chemical Engineering, Washington University in St. Louis (WUSTL), One Brookings Drive, Campus Box 1180, St. Louis, MO 63130, USA. Fax: +1 314 935 7211.
E-mail address: dudu@seas.wustl.edu (M.P. Dudukovic).

0021-9517/$ - see front matter © 2009 Elsevier Inc. All rights reserved.
doi:10.1016/j.jcat.2009.06.008

Nomenclature

A	cross sectional area of micro-reactor (m^2)
a_i	absolute calibration factor (moles/Mv)
C_i	bulk concentration of species i (moles/m^3)
c_i	pulse-normalized bulk concentration
D	diffusivity (m^2/s)
D_{e_i}	effective diffusivity in the intra-particle space defined as $D_{e_i} = \frac{\varepsilon_p}{\zeta_p} D_{T_i}$ (m^2/s)
D_{K_i}	effective Knudsen diffusivity (m^2/s)
D_{MS_i}	Maxwell–Stefan diffusivity (m^2/s)
D_{T_i}	Fickian diffusivity (m^2/s)
E_a	activation energy (kJ/moles)
$E_i(t)$	time dependent intensity measured by the mass spectrometer (Mv/s)
$F_i(t)$	exit molecular flow (moles/s)
$F_i^*(t)$	dimensionless exit flow
f_i	fugacity (Pa)
ΔH	apparent heat of adsorption (kJ/moles)
J_i	molar flux of species i (moles/m^2 s)
k_{a_i}	adsorption constant (m^3/moles s)
k_{d_i}	desorption constant (1/s)
$k_{d_i}^*$	dimensionless desorption constant
K_{eq_i}	dimensionless equilibrium adsorption constant
L	micro-reactor length (m)
Mw_i	molecular weight of species i (kg/moles)
M_j	jth moment
N_i	number of moles
q_i	adsorbed phase concentration (moles/m^3)
q_{max}	maximum concentration of adsorption sites (moles/m^3)
R	universal gas constant (kJ/moles K)
R_p	zeolite particle radius
$\bar{r}$	mean inter-particle distance (m)
T	temperature (K)
t	observation time (s)
$\bar{t}$	mean of the dimensionless response curve
$\langle x^2(t) \rangle$	mean square displacement

Greek letters

θ_i	dimensionless surface coverage or fraction surface coverage
$\overline{\theta_i}$	pulse-normalized surface coverage
$\delta^*(\tau)$	pulse-normalized delta function defined as $\delta^*(\tau) = \frac{\varepsilon_b L^2}{D_{K_i}} \delta(t)$
τ	dimensionless time
τ_{p_i}	$\frac{L^2/D_{K_i}}{R_p^2/D_{e_i}}$
μ_i	chemical potential of species i
Γ	thermodynamic correction factor
ξ	dimensionless spatial distance within the micro-reactor
η	dimensionless spatial distance within the zeolite particle
ε_b	solid holdup
ε_p	zeolite particle porosity
ζ_p	particle tortuosity
σ^2	variance of the dimensionless response curve

and do not have the resolution required for the investigation of small zeolite particles.

The temporal analysis of products (TAPs) pulse response experiment is a fast and reproducible technique which in principle can be applied to study intra-particle diffusivity and adsorption/desorption dynamics in zeolites [34,35]. In TAP pulse response experiments a small number of probe molecules are introduced as a pulse of very short duration into a micro-reactor maintained under high vacuum (10^{-8} torr). There is no continuous flow of a carrier stream, and under high vacuum conditions the external mass transfer resistance is absent. Furthermore, the low concentration of the probe molecules in the micro-reactor causes negligible thermal effects due to sorption, and the zeolite particles are easily maintained at isothermal conditions. This study uses the single pulse TAP response experiment to estimate intra-particle diffusivity and adsorption–desorption constants in commercially available beta and USY zeolites. Single pulse TAP experiments are performed using n-butane, isobutane, and argon as probe molecules (each 99.9% purity). The use of n-butane and isobutane further explores the shape-selective nature of the two zeolites. Argon, a noble gas, is inert on the surface of these zeolites and provides information on transport in the inter- and intra-particle voids. TAP reactor models that account for the adsorption, desorption and intra-particle diffusion resistances offered by the zeolite particles are presented and solved numerically. Sensitivity analysis of model predictions is conducted to determine the range of conditions under which reliable estimate of the desired adsorption–desorption and diffusion parameters can be obtained.

2. Method

A detailed description of the TAP technique and its versatility for investigating catalyst properties and reaction kinetics can be found in the literature [34–37]; only a brief description of the experimental technique is given here. The experimental TAP system [36] consists of an external high speed pulsing valve, and high vacuum chambers that house a packed-bed micro-reactor, and a computer-controlled quadruple mass spectrometer. In the single pulse mode of operation, a small number of probe molecules (10^{14} to 10^{18} molecules/pulse) are pulsed for a short interval (<100 μs) at the entrance of the micro-reactor, and the probe molecules are evacuated at the other end. After exiting the micro-reactor, the probe molecules pass through the detector of a mass spectrometer located at the exit of the micro-reactor. The mass spectrometer is set at the atomic mass unit of the desired probe species so that the actual values of the atomic mass unit t is recorded in real time as intensity ($E_i(t)$). The response curve obtained from each single pulse experiment contains the coded histories of the modes of interaction experienced by the probe molecules while traveling through the micro-reactor. Then, the response curve is generated by the appropriate theoretical model to extract quantitative information [34,35,37–39] by matching it to the experimental one.

The micro-reactor can be packed in different configurations. The simplest configuration is a one zone TAP reactor, where a measured amount of zeolite particles is packed in the reactor. Two screens, one at each end of the zeolite bed, hold the zeolite particles in place. The use of small zeolite particles in such single zone TAP reactor increases the bed resistance and causes the response curve to broaden, hence decreasing the signal to noise ratio [38]. To overcome this, a thin zone reactor configuration [37] is used. A very small amount of zeolite particles is now sandwiched between two inert zones containing larger non-porous quartz particles. This enables the use of small zeolite particles avoiding high bed resistance and insures isothermality. In this study, the zeolite particles (mass = 5 mg, diameter ~5 μm) are packed between two inert zones of non-porous quartz particles (mass = 800 mg,

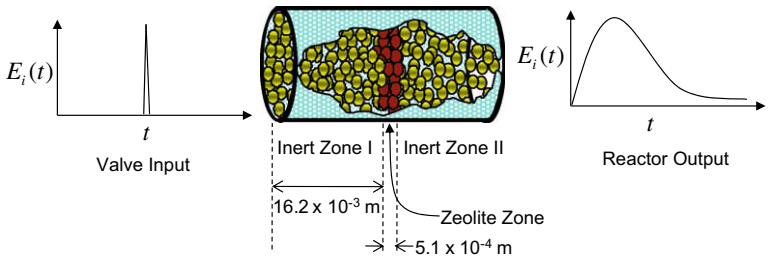

Fig. 1. Pictorial representation of single pulse TAP response experiments. Thin zeolite zone is sandwiched between two inert zones of non-porous quartz particles.

diameter ~200 μm) in the micro-reactor of length = 33×10^{-03} m, and diameter = 5×10^{-03} m, as indicated in Fig. 1. The lengths of inert zones I and II are 16.2×10^{-03} m each, and the length of the thin active zeolite layer is 5.1×10^{-04} m.

The beta and USY zeolites used in our experiments were obtained from GRACE Davison. The beta zeolite (SMR 5-9858-01062) has a Si/Al ratio of 13, and the USY zeolite (SMR 5-9858-01061) has a Si/Al ratio of 3. The beta zeolite framework consists of straight 12-membered-ring channels of free aperture 0.66×0.71 nm, viewed along axis [100] and [010] and zigzag 12-membered-ring channels of free aperture 0.56×0.56 nm, viewed along axis [001] [34]. The USY zeolite framework consists of 12-member-ring channels of free aperture 0.74×0.74 nm viewed along axis [111], and a super cage of free apertures of 1.23×1.23 nm [40]. The chemical composition and basic physical properties of both zeolites are shown in Table 1. As indicated by SEM, the average particle size of beta zeolites is ~5 μm (see Fig. 2a) and the average crystal size is ~0.3 μm (see Fig. 2b) while the average particle size of USY zeolites is ~5 μm (see Fig. 3a) and the average crystal size is ~0.25 μm (see Fig. 3b). The zeolites under investigation are calcined in situ in the micro-reactor at 673 K for 60 min. After calcination pretreatment, the zeolite is cooled to the desired temperature.

3. Theory

The flow of probe molecules in the evacuated micro-reactor is initiated by the pulse valve, and that flow lasts until all the molecules introduced in the pulse are evacuated from the reactor. Based on kinetic gas theory, at 10^{-8} torr and 373 K the mean free path lengths (λ) of argon, *n*-butane and isobutane are 0.63×10^4 m, 0.32×10^4 m, and 0.26×10^4 m, respectively. In comparison, the mean size of passages between the particles packed ($\bar{r}$) in the micro-reactor is 1.33×10^{-4} m, calculated for a particle size of 2×10^{-4} m. This indicates that the frequency of collision between probe molecules and the particles packed in the micro-reactor is at least 8 orders of magnitude higher than the frequency of collision between two probe molecules. As a result, the Knudsen regime prevails in the micro-reactor as previously established [41]. In the Knudsen regime the mean free path of a molecule is not limited by the nearby molecules but by the reactor size and size of passages between the packed particles. Knudsen diffusivity is given by [36]

$$D_K = \frac{2\varepsilon_b \bar{r}}{3\varsigma_p}\sqrt{\frac{8RT}{\pi Mw}}. \quad (1)$$

Here, $\bar{r}$ is the mean inter-particle distance or mean size of passages between the packed particles, which for spherical particles with mean particle radius R_p can be calculated as

$$\bar{r} = \frac{2\varepsilon_b}{3(1-\varepsilon_b)}R_p. \quad (2)$$

Table 1
The chemical composition and basic physical properties of beta and USY zeolites.

Properties	Beta	USY
Si/Al ratio (moles/moles)	13.3	2.90
Average crystal size (μm)	0.30	0.25
Average agglomerate size (μm)	0.50	0.50
Total surface area (m^2/g)	605	665
Surface area with pores <0.2 nm (m^2/g)	542	610
Surface area with pores >0.2 nm (m^2/g)	64	55
Total pore volume (cc/g)	0.286	0.312
Pore volume with pores <0.2 nm (m^2/g)	0.222	0.251
Pore volume with pores >0.2 nm (m^2/g)	0.064	0.061
Acidity (μmole NH_3/g catalyst)	291	466

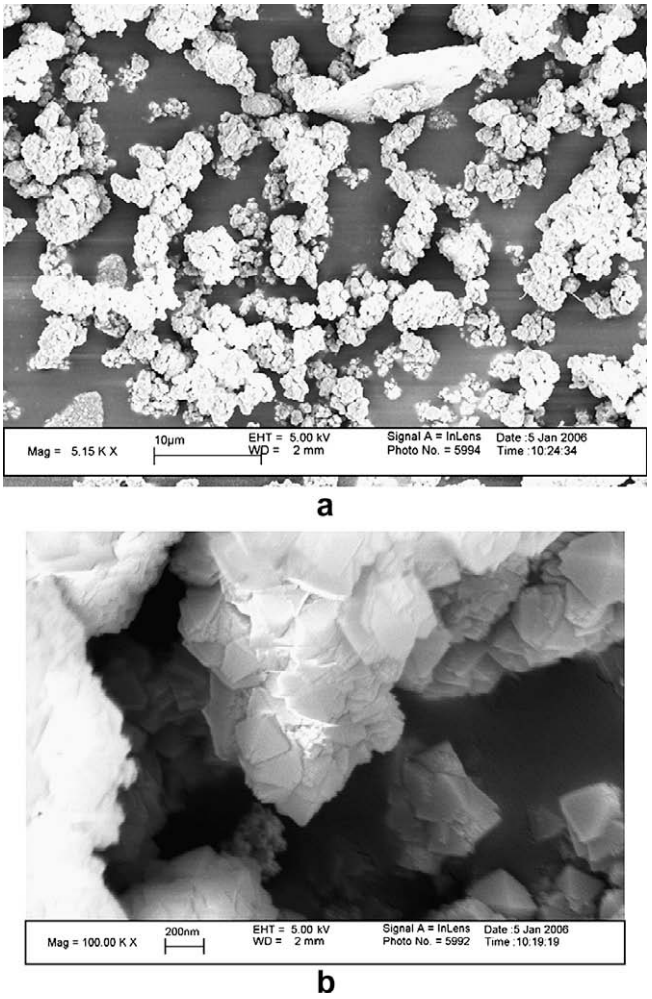

Fig. 2. SEM images (a) showing particle size distribution and (b) showing the crystallites of beta zeolite.

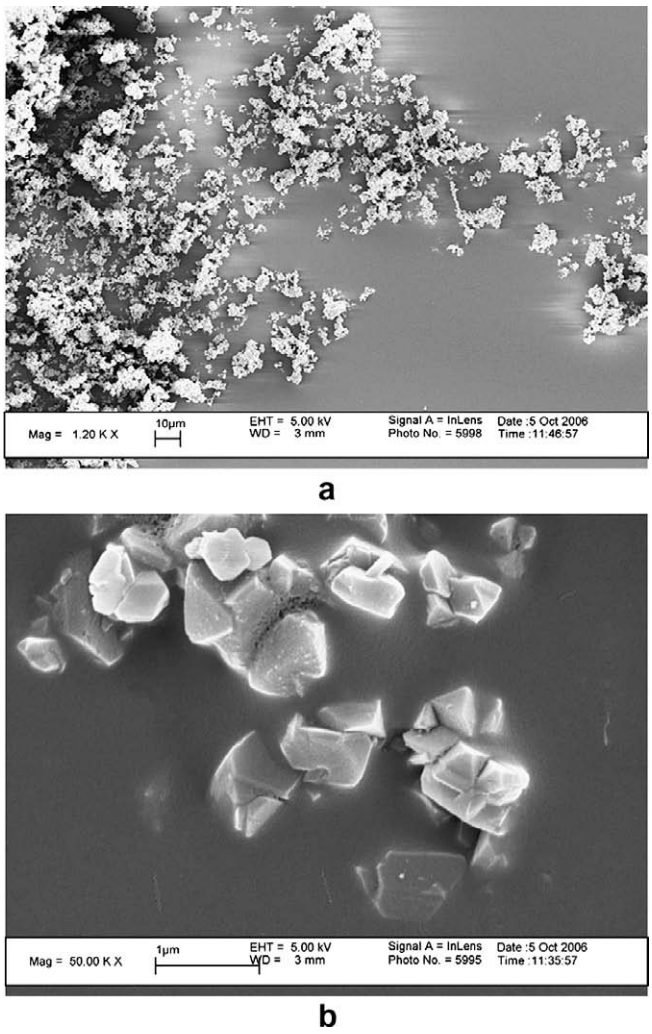

Fig. 3. SEM images (a) showing particle size distribution and (b) showing the crystallites of USY zeolite.

3.1. Inert zone model

The thin zone TAP micro-reactor shown in Fig. 1 consists of two inert zones packed with quartz particles and a thin active layer of zeolite particles sandwiched between them. In the Knudsen flow regime, the equation of continuity for inert (non-reacting) probe molecules in the inert zone is [36]:

$$\varepsilon_b \frac{\partial C_i}{\partial t} = D_{K_i} \frac{\partial^2 C_i}{\partial z^2}. \tag{3}$$

Here, C_i is the bulk concentration of species i, D_{K_i} is the effective Knudsen diffusivity of species i, t is time, z is axial position in the micro-reactor, and ε_b is the bed porosity. The dimensionless bulk concentration defined as $c_i = \frac{C_i}{N_i/AL\varepsilon_b}$ is a pulse-normalized bulk concentration. The dimensionless micro-reactor position and dimensionless time are defined as $\xi = \frac{z}{L}$, and $\tau = \frac{D_{K_i} t}{\varepsilon_b L^2}$, respectively. In dimensionless form, Eq. (3) becomes:

$$\frac{\partial c_i}{\partial \tau} = \frac{\partial^2 c_i}{\partial \xi^2}. \tag{4}$$

The dimensionless initial condition for Eq. (4) is [36,39]

$$c_i(0, \xi) = 0. \tag{5a}$$

Further, the dimensionless inlet and outlet boundary conditions are [36,39]

$$\left.\frac{\partial c_i(\tau, \xi)}{\partial \xi}\right|_{\xi=0} = -\delta^*(\tau) \quad \text{and} \tag{5b}$$

$$c_i(\tau, 1) = 0. \tag{5c}$$

Here, $\delta^*(\tau)$ is the pulse-normalized Dirac delta function defined in the nomenclature. The flux at the inlet of the mico-reactor is non-zero (Dirac pulse) for a small time (<100 μs pulse duration time) and zero otherwise This (Eq. (5b)) represents the pulse injection which occurs between the opening and closing of the pulse valve [39]. The boundary condition at the reactor outlet (Eq. (5c)) reflects the fact that it is maintained under vacuum and that the concentration of probe molecules there is almost zero. In a three-zone TAP system the continuity of concentration and flux at the boundaries between zones must be maintained. Additional description of the boundary conditions can be found in Zou et al. [39]. Eqs. (3) and (5a–c) are used to represent the inert zones I and II.

3.2. Zeolite zone model

In the thin zeolite zone, besides inter-particle diffusion, one must account for additional phenomena taking place within the zeolite particles. These are adsorption/desorption of the probe molecules on the active sites on the zeolite surface and diffusion into the zeolite pores [34,35]. Because the TAP experiments are carried out under high vacuum conditions the mass transfer in the mesopores and macropores of the zeolite particles (pore diameter >2 nm), i.e. in the inter-crystalline space, also obeys Knudsen law. However, the diffusional resistance offered by mesopores and macropores is negligible (pore diameter >0.2 nm) compared to the diffusion resistance in the nanopore space (pore diameter <2 nm), since the mean pore radius is order of magnitudes larger in the mesopores and macropores than in the nanopores. In addition, the combined mesopore and macropore surface areas contribute only 10.5% and 8.3% to the total surface areas of beta and USY zeolite, respectively (refer to Table 1). The combined pore volumes of mesopores and macropores contribute only 22.3% and 19.6% to the total pore volumes of beta and USY zeolite, respectively (refer to Table 1) and contribute less than 0.5% to the total inter-particle void volume. As a result any resistance (time constant) due to mesopores or macropores cannot be dominant, and clearly investigations under high vacuum conditions are well suited to address and attempt to quantify the resistances related to the small zeolite particles. The equation of continuity, given the low surface coverage in the inter-particle space of the thin zeolite zone, is

$$\varepsilon_b \frac{\partial C_i}{\partial t} = D_{K_i} \frac{\partial^2 C_i}{\partial z^2} - (1 - \varepsilon_b) q_{\max} \left[k_{a_i} C_i - k_{d_i} \theta_i\right]\big|_{r=R_p}. \tag{6}$$

Here, θ_i is the dimensionless surface coverage defined as $\theta_i = \frac{q_i}{q_{\max}}$. The second term on the right-hand side of Eq. (6) represents the net flux of probe molecules into the zeolite particles, from the bulk gas phase to the surface of the zeolite particles, and is given as the net rate of adsorption on the outside zeolite surface.

To complete the model one must describe the behavior within the zeolite particles. At the zeolite surface it is assumed that the probe molecules first adsorb reversibly. Then the adsorbed molecule either diffuses inside the particle or it desorbs from the surface (see Fig. 4). Within the nanopores the diffusing species in nanoporous zeolites never leave the force field of the pore walls [42]. Hence, the molecules within the pores can be regarded as a single "adsorbed" phase [25]. Thus, the true driving force for diffusion is the gradient in the chemical potential, rather than the gradient of concentration, as is assumed in Fick's formulation. Hence, a correction factor is used to relate Fickian diffusivity or transport diffusivity (D_{T_i}) to the intrinsic or Maxwell–Stefan diffusivity (D_{MS_i}) and the relationship is given as $\frac{D_{T_i}}{D_{MS_i}} = \Gamma$ [43,44]. Here, Γ is the

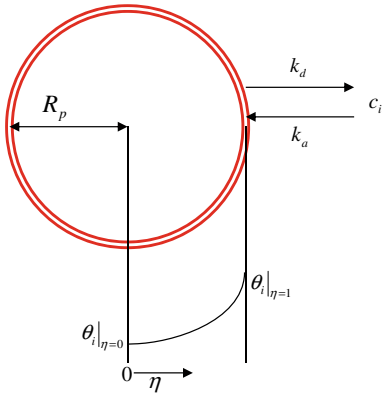

Fig. 4. Pictorial representation of sorption processes on zeolite boundary and transport in zeolite's intra-particle space.

thermodynamic correction factor, defined as $\Gamma = \theta_i \frac{\partial \ln f_i}{\partial \theta_i} = \frac{\partial \ln f_i}{\partial \ln \theta_i}$. In the limit of zero surface coverage ($\theta_i \to 0$), the Fickian and Maxwell–Stefan diffusivities are identical ($D_{T_i} = D_{MS_i}$) and the thermodynamic correction factor is unity ($\Gamma = 1$) [44]. This is normally the case under TAP experimental conditions, as the number of molecules in a single pulse is typically much smaller (1000 to 1,000,000 times) than the number of active sites in the zeolite particles.

The one-dimensional flux under the limit of zero surface coverage for a single component diffusing from the exterior surface to the center of a spherical zeolite crystal with radius R_p, is thus given as [43]

$$J_i = -q_{\max} D_{T_i} \frac{d\theta_i}{dr}, \quad \theta_i \to 0, \tag{7}$$

and the mass balance in the intra-particle space is

$$\frac{\partial \theta_i}{\partial t} = D_{e_i} \left[\frac{\partial^2 \theta_i}{\partial r^2} + \frac{2}{r} \frac{\partial \theta_i}{\partial r} \right]. \tag{8}$$

Eqs. (6) and (8) can be transformed into dimensionless form as

$$\frac{\partial c_i}{\partial \tau} = \frac{\partial^2 c_i}{\partial \xi^2} - (1 - \varepsilon_b) k^*_{d_i} \left[K_{eq_i} c_i - \overline{\theta_i} \right] \Big|_{\eta=1} \tag{9}$$

and

$$\frac{\partial \overline{\theta_i}}{\partial \tau} = \tau_{p_i} \left[\frac{\partial^2 \overline{\theta_i}}{\partial \eta^2} + \frac{2}{\eta} \frac{\partial \overline{\theta_i}}{\partial \eta} \right]. \tag{10}$$

The dimensionless boundary conditions for Eq. (10) at the zeolite exterior surface and at the center are given as

$$\left. \frac{\partial \overline{\theta_i}}{\partial \eta} \right|_{\eta=1} = \left. \frac{k^*_{d_i}}{3\tau_{p_i}} \left[K_{eq_i} c_i - \overline{\theta_i} \right] \right|_{\eta=1} \tag{11a}$$

and

$$\lim \left(\eta \frac{\partial \overline{\theta_i}}{\partial \eta} \right) \Big|_{\eta=0} = 0. \tag{11b}$$

Here, $\overline{\theta_i}$ is the pulse-normalized dimensionless surface coverage, analogous to the pulse-normalized dimensionless bulk concentration (c_i). It is the ratio of the concentration of sites occupied by the adsorbing species, q_i, and the bulk concentration in the micro-reactor that would result if all the molecules introduced by the pulse valve were distributed instantaneously throughout the inter-particle space in the micro-reactor. It is the product of the dimensionless surface coverage $\theta_i = \frac{q_i}{q_{\max}}$ and the ratio of the maximum concentration of adsorption sites to the pulse intensity, and it is defined as $\overline{\theta_i} = \theta_i \frac{q_{\max}}{N_i/AL\varepsilon_b}$. The dimensionless particle time τ_{p_i}, dimensionless desorption constant $k^*_{d_i}$, and dimensionless equilibrium adsorption constant K_{eq_i} for species i are the three dimensionless constants of the developed model defined as

$$\tau_{p_i} = \frac{L^2/D_{K_i}}{R_p^2/D_{e_i}} = \frac{\text{Characteristic diffusion time in micro} - \text{reactor}}{\text{Characteristic diffusion time in zeolite pore}}, \tag{12}$$

$$k^*_{d_i} = \frac{L^2/D_{K_i}}{1/k_{d_i}} = \frac{\text{Characteristic diffusion time in micro} - \text{reactor}}{\text{Characteristic desorption time}}, \tag{13}$$

and

$$K_{eq_i} = q_{\max} \frac{1/k_{d_i}}{1/k_{a_i}} = \frac{\text{Characteristic desorption time}}{\text{Characteristic adsorption time}}. \tag{14}$$

Eqs. (3), (5a–c), (9), (10) and (11a and b) describe the thin zone reactor configuration and different interactions taking place within the zeolite particles. The three dimensionless constants τ_{p_i}, $k^*_{d_i}$, and K_{eq_i} affect the shape, peak position and height of the model simulated response curve. Attempts were made to reduce the model to a two-parameter model (τ_{p_i} and K_{eq_i}) by assuming that the bulk concentrations inside and outside the zeolite pores are in pseudo-equilibrium [34,38,45]. If in addition one assumes that the nanopore diffusion is not the rate limiting step, then the model is reduced to only one dimensionless constant, K_{eq_i} [45]. In this study no such assumptions are made, as our goal is to investigate the use of the single pulse TAP response experiment and of the full model in estimating intra-particle diffusivity and adsorption–desorption constants.

4. Solution procedure

4.1. Method of moments to estimate effective knudsen diffusivity

The effective Knudsen diffusivity D_{K_i} in an inert zone can be determined by either fitting in the time domain the experimental response curve with a model (Eq. (3)) generated one or by matching the moments of the predicted and measured responses. Both have been successfully employed in the past [37,39]. Moreover there is ample evidence that the response curve obeys Knudsen diffusion in an inert zone [34–37]. Recently, Feres et al.[46] have presented a stochastic model that confirmed the findings of the previous continuum-based models. The method of moments is used in this study to determine the effective Knudsen diffusivity in the inter-particle space of the TAP micro-reactor. A single effective Knudsen diffusivity for each probe molecule is sufficient to describe the inter-particle transport provided the inter-particle space in the bed has a unimodal pore size distribution. This assumption is particularly true for the thin zone TAP reactor, as more than 99% of the packed micro-reactor volume is filled with non-porous quartz particles with a mean diameter of 200 μm.

The jth moment is defined as $M_j = \int_0^\infty E(t) \times t^j dt$. Here $E(t)$ is the experimental response obtained from the TAP reactor in real time t. The mean residence time of the response curve is determined by dividing the first moment (M_1) with the zeroth moment (M_0). In the case of strictly Knudsen diffusion with diffusivity D_{K_i} in the inter-particle space the mean residence time is the characteristic diffusion time of the probe molecule under investigation in the micro-reactor. Thus, for species i, the characteristic diffusion time in the reactor is

$$\frac{L^2 \varepsilon_b}{D_{K_i}} = \frac{\int_0^\infty E_i(t) \times t dt}{\int_0^\infty E_i(t) dt}. \tag{15}$$

Here, L is the length of the TAP micro-reactor (33×10^{-03} m) and ε_b is the bed porosity (~0.5), which is measured independently.

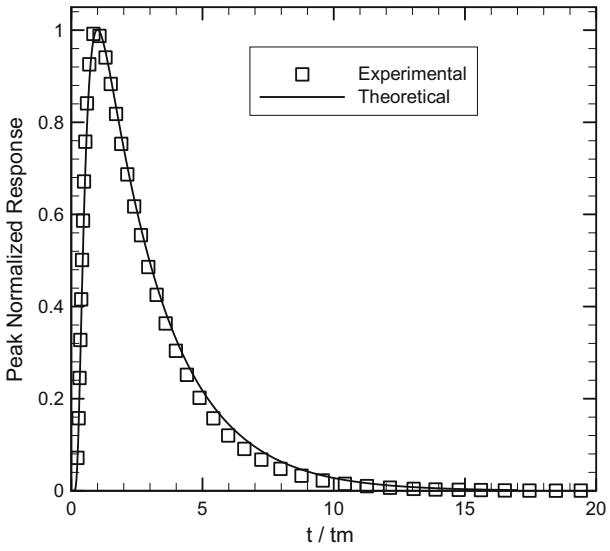

Fig. 5. Comparison of experimental peak-normalized response of argon when pulsed over the thin zone micro-reactor containing beta zeolite at 373 K and theoretical peak normalized plot.

When an inert gas like argon is pulsed into the TAP micro-reactor containing a zeolite sample, the gas molecules interact weakly on the surface of the particles (both zeolite and non-porous quartz). Olea and Iwasawa [47] found that when a single pulse of argon was introduced over the micro-porous particles (<2 nm in diameter), both inter- and intra-particle diffusion affects the response curve. As a result, both inter- and intra-particle diffusivities were needed to represent the argon response curve. These authors used the one-zone micro-reactor configuration and the experiments were performed at or near ambient temperatures (300 K). However, in the present study, the use of the thin zone micro-reactor configuration allows us to neglect the resistance of inter-particle diffusion in the zeolite zone, as the total pore volume of both beta and USY zeolite particles contributes less than 1% to the total inter-particle void volume. The assumption that only Knudsen diffusivity in the inter-particle voids affects the argon response curve was verified by comparing the experimental peak-normalized response to the theoretical peak-normalized plot [36]. The experimental peak-normalized response curve is obtained by dividing the experimental response with the peak magnitude and plotting it as a function of (t/t_m), where t_m is the time at which the maximum occurs. The theoretical peak-normalized plot is obtained from the series solution of the continuity equation assuming only Knudsen diffusion in the inter-particle void [36]. Fig. 5 shows the comparison of the experimental peak-normalized response of argon when pulsed over the thin zone micro-reactor containing beta zeolite at 373 K with the theoretical peak normalized plot. A good match is found between the experimental and model predicted peak-normalized plots. Similar results are also found for the temperature range used in this study and when argon is pulsed over the micro-reactor with a thin zone of USY zeolite (these results are not shown here for brevity). Hence, argon is used to estimate the effective Knudsen diffusivity in the inter-particle voids.

The effective Knudsen diffusivity of any other probe molecule is then computed by using the known temperature and molecular weight dependence of Knudsen diffusivity which is $D_{K_i} \propto \sqrt{T/Mw_i}$. To verify this dependency under TAP experimental conditions single pulses of argon and isobutane are introduced into the evacuated micro-reactor packed with inert particles (non-porous quartz) at various temperatures. The experiments are repeated to check for the reproducibility of the experimental data. The characteristic diffusion times in the micro-reactor for each pulse are calculated from the method of moments approach, as shown in Eq. (15). It is found that the relative error of the characteristic diffusion time in the micro-reactor for each pulse of argon and isobutane at each temperature is less than 2.5%. In the non-porous quartz bed, at temperatures above ambient, both argon and isobutane interact only weakly on the surface of the particles and the characteristic diffusion time of the micro-reactor reflects only the transport process in the inter-particle voids which has been established to be Knudsen diffusion [34–36].

Fig. 6 shows the characteristic diffusion times in the micro-reactor for isobutane and argon, divided by the square root of their respective molecular weights $\frac{L^2\varepsilon_b}{D_{K_i}}\Big/\sqrt{Mw_i}$, as a function of the inverse square root of temperature. Fig. 6 clearly demonstrates that the characteristic diffusion times of isobutane and argon in the micro-reactor follow the square root of temperature and square root of molecular weight dependencies in the given temperature range.

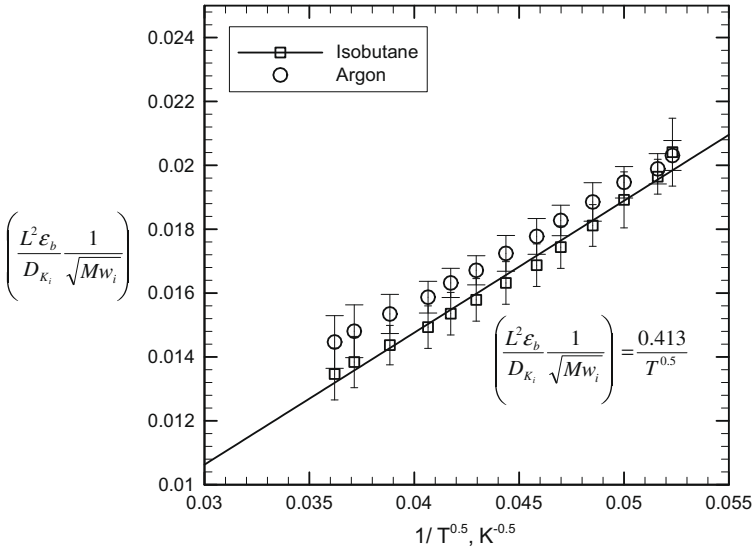

Fig. 6. The characteristic diffusion times in the micro-reactor of isobutane and argon, divided by the square root of their respective molecular weights, as a function of the inverse square root of temperature. The micro-reactor was packed with non-porous quartz particles (total mass = 800 mg and mean diameter = 200 μm).

Furthermore, extrapolating the line that connects all the experimental data points in Fig. 6 leads to zero intercept on the ordinate, as it should, and the line has a positive slope of unity. This confirms that the inter-particle transport in the TAP micro-reactor can be characterized as Knudsen diffusion.

Consequently, in this study for a thin zone TAP micro-reactor packed with beta or USY zeolite the effective Knudsen diffusivities in the inter-particle voids for isobutane and *n*-butane are estimated from argon response curve.

4.2. Numerical technique and minimization procedure to estimate dimensionless constants (τ_{p_i}, K_{eq_i}, and $k^*_{d_i}$)

After the effective Knudsen diffusivity of each probe molecule is independently quantified, the dimensionless constants, τ_{p_i}, K_{eq_i}, and $k^*_{d_i}$ for – adsorbing molecules are estimated by fitting the dimensionless exit flux obtained from a single pulse TAP experiment with the numerically calculated dimensionless exit flux. Here the dimensionless exit flux is defined as $F^*_i = \frac{\partial c_i(\tau,\xi)}{\partial \xi}\Big|_{\xi=1}$. The experimental dimensionless exit flux is obtained by relating the count intensity from the mass spectrometer to the molecular flow. The detailed mathematical treatment of the mass spectrometer count intensity to obtain the dimensionless exit flux is explained in Section 4.3. Here the minimization procedure and numerical techniques used to solve the governing equations are discussed.

The governing equations for the TAP micro-reactor and zeolite particles are second-order PDEs numerically solved by using the method of lines [48]. The method relies on the approximation of spatial derivatives, reducing partial differential equations (PDEs) to sets of ordinary differential equations (ODEs). The resulting ODEs are solved using stiff ODE solvers from NETLIB libraries.

To estimate the parameters we used ODRPACK public domain software for minimizing the sum of the square weighted orthogonal distances from the experimental data to a curve or surface. Using this method, the orthogonal distance between the experimental exit flux and modeled exit flux is minimized for every time step by changing the parameters. A detailed discussion about the algorithm, its stability, efficiency, and advantage over the ordinary least squares method, especially in the case of nonlinear problems, can be found elsewhere [49].

4.3. Mathematical treatment of TAP experimental data

As mentioned earlier, the molecule count ($E_i(t)$) emerging from the exit of the micro-reactor is recorded in real time using a computer-controlled quadruple mass spectrometer. To obtain quantitative information, the time dependent intensity ($E_i(t)$) measured by the mass spectrometer is related to the molecular flow ($F_i(t)$) at the exit of the micro-reactor. In a single pulse TAP experiment, the intensity of an experimental response is proportional to the exit molecular flow, and the relationship is given by

$$F_i = a_i E_i(t). \tag{16}$$

Here, a_i is the absolute calibration factor for species *i*, $E_i(t)$ is the experimental response curve, and F_i is exit molecular flow (moles/s) of species *i*. The dimensionless exit flow F^*_i is given as

$$F^*_i = \frac{F_i}{N_i}\frac{\varepsilon_b L^2}{D_{K_i}}. \tag{17}$$

Integrating Eq. (17) with respect to time, we obtain

$$\int_0^\infty F_i dt = a_i \int_0^\infty E_i dt,$$

or

$$a_i = \frac{\int_0^\infty F_i dt}{\int_0^\infty E_i dt}. \tag{18}$$

For a probe species involved in a reversible process (as in this study) or for a non-reacting probe species, the integration of the exit flow with respect to time yields the number of moles of probe species *i* injected in the system:

$$\int_0^\infty F_i dt = N_i. \tag{19}$$

So Eq. (18) can be rewritten as

$$a_i = \frac{N_i}{\int_0^\infty E_i dt}. \tag{20}$$

Thus, the time dependent intensity ($E_i(t)$) measured by the mass spectrometer is related to molecular flow ($F_i(t)$) at the exit of the micro-reactor as

$$F_i = \frac{N_i}{\int_0^\infty E_i dt} E_i, \tag{21}$$

and the dimensionless exit flow F^*_i can be rewritten as

$$F^*_i = \frac{E_i}{\int_0^\infty E_i dt}\frac{\varepsilon_b L^2}{D_{K_i}}. \tag{22}$$

5. Results and discussion

5.1. Comparison of response curves obtained from single pulse tap experiments

Fig. 7 shows the comparison of the dimensionless experimental response curves of isobutane and *n*-butane obtained when pulsed over the micro-reactor with the thin zone of beta or USY zeolite at 423 K. It is observed that the shape of the isobutane and *n*-butane response curve is similar indicating that the difference in transport and adsorption–desorption phenomena for isobutane and *n*-butane in beta zeolite are negligible, and beta zeolite has a similar affinity toward both branched and straight chain C_4 alkanes. This similarity is observed for all temperatures investigated in this study.

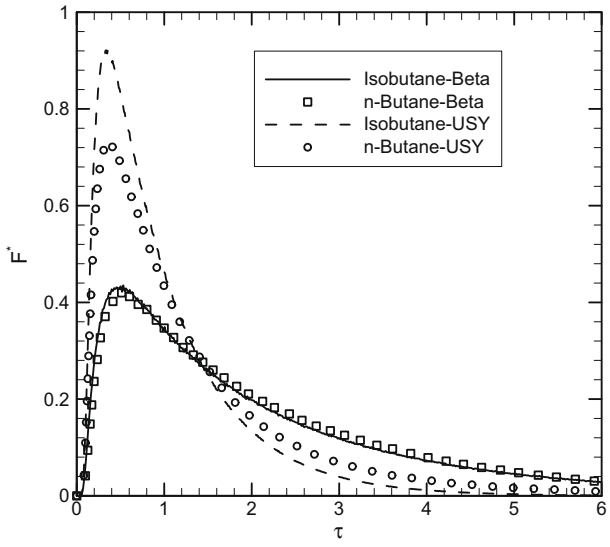

Fig. 7. Comparison of the dimensionless experimental response curves of isobutane and *n*-butane obtained when pulsed over thin zone of beta or USY zeolite at 423 K.

In the case of USY zeolite it is observed that the magnitude of the peak for isobutane compared to that for *n*-butane is larger and the elution time for *n*-butane response curve is much longer than the one for isobutane. This indicates that in USY zeolite both the nanopore transport and adsorption–desorption are faster for isobutane than for *n*-butane. Hence, USY zeolite has stronger affinity for adsorbing straight chain C_4 alkanes. This property of USY zeolite can be used for selective separation of straight C_4 alkanes.

For both isobutane and *n*-butane at a given temperature the USY response curve peak appears sooner than on the beta zeolite and the curve exhibits a generally shorter elution time than the one for beta zeolite. These differences indicate that the characteristic nanopore diffusion and characteristic desorption times are faster in USY zeolite than in beta zeolite and this may be caused due to the larger pore diameter and smaller crystal size of USY zeolite.

5.2. Sensitivity analysis of dimensionless constants

In transient experimental techniques such as TAP, only certain ranges of nanopore diffusion and adsorption–desorption constants can be determined [34,35,45]. Keipert and Baerns [34] found the intra-crystalline diffusivity range within which its values affect the shape of the TAP response curves. They did this by simulating the response curves for varied intra-particle diffusivities while other parameters were maintained constant. A similar approach is adopted in this study. In the model the three dimensionless constants τ_{p_i}, K_{eq_i}, and $k^*_{d_i}$ affect the shape of the TAP response curve. Simulations were carried out at τ_{p_i}, K_{eq_i}, and $k^*_{d_i}$ of different orders of magnitudes to discriminate between the time scales of intra-particle diffusion, adsorption–desorption, and inter-particle diffusion. The mean and variance of the simulated response curves were calculated to find the ranges of τ_{p_i}, K_{eq_i}, and $k^*_{d_i}$ within which the response curve is sensitive to their values. Here, the mean and variance of the response curve are defined as

$$\overline{\tau} = \frac{\int_0^\infty F_i^*(\tau) \times \tau d\tau}{\int_0^\infty F_i^*(\tau) d\tau}, \tag{23}$$

and

$$\sigma^2 = \frac{\int_0^\infty F_i^*(\tau) \times \tau^2 d\tau}{\int_0^\infty F_i^*(\tau) d\tau} - \overline{\tau}^2. \tag{24}$$

Fig. 8a and b display some of the calculations performed and clearly establish that asymptotic values of the moments of the response at some very small or very large parameter values preclude reliable estimates of these constants. These parametric sensitivity studies established that the above-mentioned constants must be in the ranges indicated in Table 2 for the reliable estimation of various parameters to be possible. Since the values of these dimensionless groups cannot be known 'a priori', this implies that proper estimation of system parameters by TAP will require an iterative approach. The values of the dimensionless constants have to be first estimated based on prior experience and the experiment designed based on these estimates so as to ensure that these constants fit in the ranges indicated in Table 2. Upon processing the experimental results if some constants were found outside the permissible range, the experiment should be redesigned to bring them into range. Unfortunately, we did not have access to the TAP equipment long enough to complete this iterative process and thus report only the results obtained with the original experiment design described earlier.

As an illustration of the physical reasoning as to why certain parameters cannot always be estimated from the TAP response curve, consider the range of the dimensionless τ_{p_i} which is the ratio of the characteristic diffusion time in the micro-reactor to the characteristic diffusion time in the zeolite pores. A value of τ_{p_i} equal to unity means that the time scales for intra-particle and inter-particle diffusion are the same, and that the characteristic diffusion time in the zeolite particle is not a rate limiting parameter. In this limiting case, the concentration gradient in the intra-particle space is negligible and the effective intra-particle diffusivity of adsorbed species is fast. When the effective intra-particle diffusivity of adsorbed species is very small, for example in the case of τ_{p_i} equals 10^{-6}, the difference in time scales for intra-particle and inter-particle diffusion is very large. Under this limiting case, most of the flux of the adsorbing species reaches the micro-reactor outlet before considerable diffusion can occur in the zeolite pores. Similar limitations are also observed in other the transient experiments, such as ZLC [50] and TEOM [18].

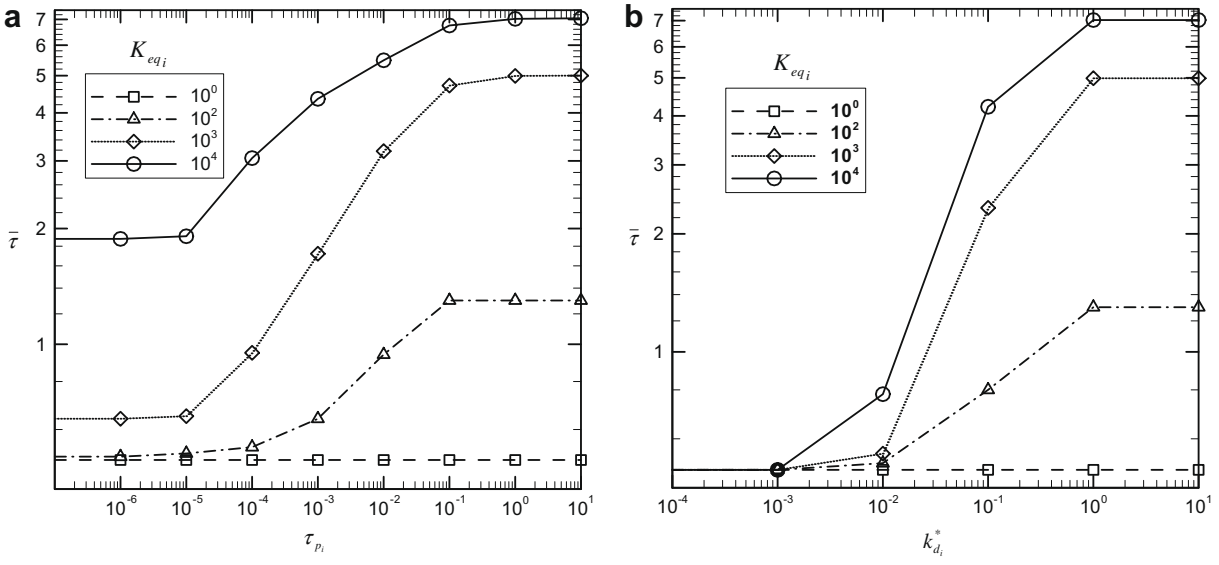

Fig. 8. Results of numerical experiments (a) calculated means ($\overline{\tau}$) of the simulated response curves as the function of dimensionless time constants τ_{p_i} and K_{eq_i} and (b) calculated means ($\overline{\tau}$) of the simulated response curves as the function of dimensionless time constants $k^*_{d_i}$ and K_{eq_i}.

Table 2
The upper and lower limits of the dimensionless parameters τ_{p_i}, K_{eq_i}, and $k^*_{d_i}$ that affect the shape of the TAP response curve.

Dimensionless time constants	Lower limit	Upper limit
τ_{p_i}	10^{-6}	10^{0}
$k^*_{d_i}$	10^{-2}	10^{0}
K_{eq_i}	10^{0}	N/A

5.2.1. Tuning experimental conditions to obtain reliable estimates

The range of dimensionless model constants reported in Table 2 indicates the parameter space within which the model can reliably estimate the quantities we are seeking, e.g. intra-particle diffusivity and adsorption–desorption constants. This range of the dimensionless constants cannot be altered; therefore the experimental conditions should be tuned so that the estimated parameters τ_{p_i} and $k^*_{d_i}$ fall within their desired ranges reported in Table 2. Accordingly the following alterations of the experimental conditions are proposed. For probe molecules with low intra-particle diffusivities, represented by the lower limit of time constant τ_{p_i}, the value of τ_{p_i} can be augmented by decreasing the zeolite particle size, by increasing the micro-reactor length, or by decreasing the Knudsen diffusivity in the inter-particle voids in the bed by using smaller inert particles in the micro-reactor. In contrast, for fast diffusing probe molecules in the intra-particle space, represented by the upper limit in the permissible range, the lower value of τ_{p_i} is achieved by doing exactly the opposite. Similarly, by altering the micro-reactor length and Knudsen diffusivity in the inter-particle void, the experiments can be tuned so that $k^*_{d_i}$ falls within the required range. These alterations in the experimental conditions should provide guidance for future single pulse TAP experiments to obtain reliable estimates of intra-particle diffusivity and adsorption–desorption constants.

5.3. Comparison of experimental and simulated tap response curve

The simulated TAP response curves were fitted to the experimentally obtained ones by adjusting the three model parameters τ_{p_i}, K_{eq_i}, and $k^*_{d_i}$. Experiments were carried out at various temperatures. A mass balance check was made for the conditions of each run to ensure that there was no reaction or irreversible adsorption of the probe molecules on the zeolite surface. This check consisted of comparing the number of molecules exiting the micro-reactor (zeroth moment (M_0)) containing the thin zone of zeolite with

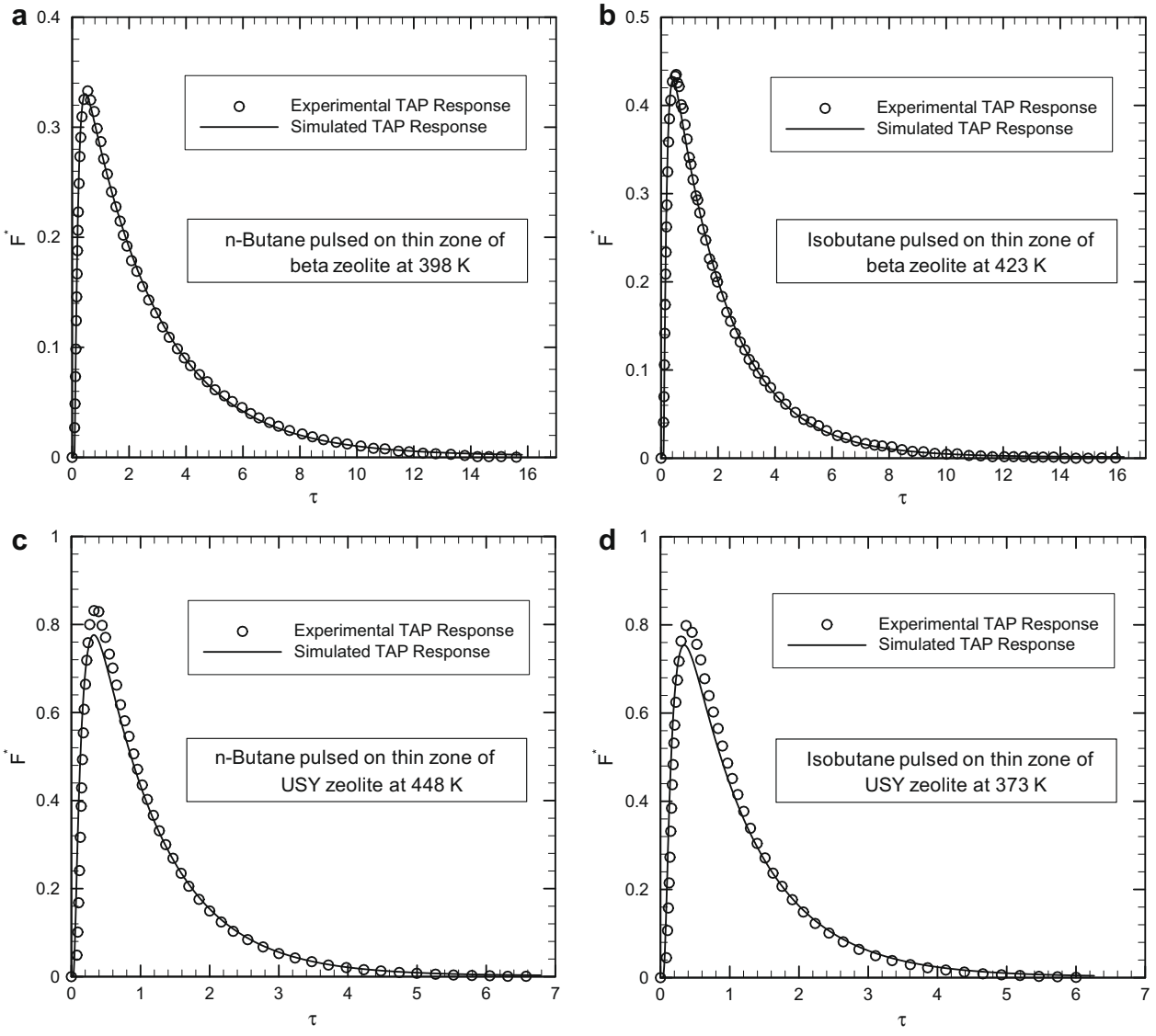

Fig. 9. Comparison between the simulated and experimental dimensionless exit flux of isobutane and *n*-butane as a function of dimensionless times at selected temperatures.

the response of the same micro-reactor packed only with non-porous quartz, for the same input pulse intensity.

5.3.1. Beta zeolite

Fig. 9a and b compare the simulated and experimental dimensionless exit flux $\left(F_i^* = \frac{\partial c_i(\tau,\xi)}{\partial \xi}\Big|_{\xi=1}\right)$ of isobutane and *n*-butane as a function of dimensionless times (τ) at selected temperatures. The experimental F_i^*, obtained from single pulse TAP experiments, where beta zeolite (mass = 5 mg and mean diameter = 5 μm) was sandwiched between two inert zones (non-porous quartz, mass = 800 mg and mean diameter = 200 μm) is matched well with the developed model. Furthermore, the dimensionless parameters, τ_{p_i} and K_{eq_i}, estimated by fitting the experimental response curves with the corresponding model simulated ones, are within the appropriate sensitivity ranges shown in Table 2. However, the dimensionless desorption constant $\left(k_{d_i}^*\right)$ for isobutane and *n*-butane pulses over a thin zone of beta zeolite can only be estimated at 378 K since at higher temperatures the estimated $k_{d_i}^*$ is outside of the model sensitivity range at the current set of experimental conditions. The estimated $k_{d_i}^*$ values are shown in Table 3. At 373 K, the dimensionless constants τ_{p_i}, K_{eq_i}, and $k_{d_i}^*$ are 1.240×10^{-5}, 6268 and 0.58, respectively, for isobutane in beta zeolite. These estimated values will be beneficial to test various theories such as molecular dynamics, transition-state theory, mean-field theories and Monte-Carlo techniques, as they are obtained at low surface coverage.

5.3.2. USY Zeolite

Fig. 9c and d compare the simulated and experimental dimensionless exit flux of isobutane and *n*-butane as a function of dimensionless time at selected temperatures. The experimental F_i^* was obtained from single pulse TAP experiments conducted over thin zone of USY zeolite. Fig. 9c and d illustrate that the developed model under-predicts the dimensionless exit flux near the peak, but is in good agreement elsewhere for both isobutane and *n*-butane. Unfortunately, the dimensionless constants τ_{p_i}, and $k_{d_i}^*$ estimated by minimization procedure are found to be outside the model sensitivity range shown in Table 2. This is apparently caused by faster intra-particle diffusion and shorter desorption times observed in USY zeolite. This can be corrected in the future experiments by tuning the experimental conditions as explained in Section 5.2.1; for now only the dimensionless parameter K_{eq_i} is estimated.

5.4. Dimensionless equilibrium parameter (K_{eq_i})

The values of the dimensionless equilibrium parameter (K_{eq_i}), its standard deviation and 95% confidence interval, estimated by regressing the experimental TAP responses at different temperatures with the model simulated ones, are shown in Table 4. It is evident that on beta zeolite the estimated K_{eq_i} for branched paraffin (isobutane) is lower than straight chain (butane), however, the difference in the estimated K_{eq_i} values for isobutane and *n*-butane is minor. For example, the dimensionless K_{eq_i} value for isobutane/beta is 2480 and *n*-butane/beta is 2638 at 423 K. Similar observations were also reported in the literature, for example, the estimation of the Langmuir adsorption constants of isobutane and *n*-butane in beta zeolite by the TEOM (Tapered Element Oscillating Microbalance) method yielded 4451/bar and 4981/bar at 323 K, respectively [17]. Denayer et al. [16] reported similar behavior, however, the difference in their estimated Henry's constants for isoalkanes compared to *n*-alkanes was much higher. They investigated the C_5 to C_8 alkanes in beta zeolite using tracer and perturbation chromatographic techniques. Consequently, the number of carbon in alkanes influences the adsorption–desorption phenomena in beta zeolite.

On USY zeolite much lower estimates of K_{eq_i} are obtained for isobutane than for *n*-butane, indicating USY zeolite's stronger affinity for a straight chain paraffin, assuming that the maximum sites for the adsorption of isobutane and *n*-butane are the same. For example, dimensionless K_{eq_i} values for isobutane/USY zeolite is 802 and for *n*-butane/USY zeolite is 1177 at 423 K. A similar behavior was also reported in the literature. For example, Gong [17] estimated Langmuir adsorption constants for isobutane and *n*-butane in USY zeolites as 71 1/bar and 102 1/bar at 303 K, respectively, and Zhang et al. [24] estimated dimensionless Henry's constant for isobutane and *n*-butane in USY zeolite as 2.1 and 3.8 at 303 K, respectively. A similar behavior was also reported for C_5 alkanes [16] (Henry constant value for n-pentane/ Na-USY zeolite is 2.30×10^{-6} moles/kg Pa and 2.16×10^{-6} moles/kg Pa at 573 K, respectively). However for alkanes with carbon number C_6 to C_8 showed non-selective competitive adsorption of isoalkanes and *n*-alkanes on Na-USY zeolite [16]. Consequently, the USY zeolite shows affinity toward *n*-alkanes for alkanes with lower carbon numbers.

At this point it is instructive to point out the differences between the equilibrium constants reported in the literature, obtained by various techniques and the K_{eq_i} values obtained by TAP. The former actually calculate the equilibrium constant by dividing the experimentally determined number of molecules of adsorbed species per unit mass of the zeolite, normalized with the total

Table 3
The values of the dimensionless desorption constant $\left(k_{d_i}^*\right)$, with the standard deviation and 95% confidence interval estimated over a thin zone of beta zeolite.

Probe molecules	T (K)	$k_{d_i}^*$ ($\times 10^{-1}$)	Std. deviation ($\times 10^{-2}$)	95% Confidence interval ($\times 10^{-1}$)
Isobutane	373	5.860	1.47	5.580 to 6.151
Butane	373	2.690	0.40	2.610 to 2.770

Table 4
The values of the dimensionless equilibrium parameter (K_{eq_i}), with the standard deviation and 95% confidence interval, and apparent heats of adsorption (ΔH) obtained from van't Hoff's plot.

Probe molecules	Zeolites	T (K)	K_{eq} ($\times 10^3$)	Std. deviation ($\times 10^1$)	95% Confidence interval ($\times 10^3$)	$-\Delta H$ (kJ/mole)
Isobutane	Beta	373	6.268	7.11	6.128 to 6.400	23.6
		398	4.288	1.75	4.288 to 4.288	(s.d. 2.32)
		423	2.480	0.78	2.460 to 2.498	
		448	1.416	1.64	1.384 to 1.448	
		473	1.318	3.00	1.259 to 1.377	
		498	1.031	2.68	0.962 to 1.060	
Butane	Beta	373	7000	7.44	6.790 to 7.230	24.5
		398	3.525	1.17	3.502 to 3.548	(s.d. 2.51)
		423	2.638	4.00	2.560 to 2.716	
		448	1.451	3.81	1.376 to 1.526	
		473	1.345	1.75	1.311 to 1.380	
		498	0.990	2.37	0.943 to 1.036	
Isobutane	USY	323	2.777	2.75	2.744 to 2.811	14.12
		348	1.482	1.71	1.431 to 1.533	(s.d. 1.85)
		373	1.047	2.61	0.951 to 1.100	
		398	0.919	2.58	0.869 to 0.970	
		423	0.802	2.69	0.758 to 0.847	
		448	0.742	1.78	0.707 to 0.776	
		483	0.733	1.94	0.695 to 7.716	
Butane	USY	323	5.240	3.08	5.189 to 5.310	16.7
		348	3.689	1.58	3.658 to 3.720	(s.d. 0.80)
		373	2.239	0.80	2.223 to 2.253	
		398	1.476	0.90	1.459 to 1.494	
		423	1.177	0.60	1.165 to 1.189	
		448	0.941	1.60	0.910 to 0.973	
		483	0.788	1.56	0.757 to 0.819	

number of sites that are available per unit mass of zeolite, with the equilibrium partial pressure of the adsorbing species (hence units of atm^{-1} or bar^{-1} as quoted above appear in the literature). The important normalization factor is obtained at sufficiently high partial pressure of the adsorbing species where all sites are occupied in equilibrium. Thus these sites comprising the total possess different energies for adsorption. In contrast, in single pulse TAP experiments one does not have access to the total number of sites and the K_{eq_i} values are obtained from dynamic experiments by computing the ratio of characteristic desorption and adsorption times. The needed normalization factor represents now the total sites available for adsorption at zero coverage and could change with temperature and experimental conditions. Thus quantitative comparison of TAP obtained equilibrium constant values and those obtained by other techniques cannot be made at present. Yet TAP values are well suited for comparison with molecular dynamics calculations. Moreover the trends in the values should be comparable.

5.5. Temperature dependency of equilibrium parameter (K_{eq_i})

The temperature dependency of the obtained dimensionless equilibrium constant (K_{eq_i}) is represented by van't Hoff's equation. Fig. 10a and b display the van't Hoff plot for equilibrium constant K_{eq_i} calculated for isobutane and *n*-butane in beta and USY zeolites. The estimated apparent heat of adsorption with standard deviation is reported in Table 4. It is found that the apparent heat of adsorption estimated here is considerably lower than what is reported in the literature. For example, the heat of adsorption estimated by Gong [17] for isobutane/USY zeolite is 35 ± 4 kJ/mole compared to 14.3 (s.d. 2.3) kJ/mole estimated in this study. Similarly for butane/USY zeolite the heat of adsorption was reported as 39 ± 4 kJ/mole [17] compared to 16.3 (s.d.0.8) kJ/mole estimated in this study.

One possible reason for the discrepancy may be the influence of the carrier gas. Mittelmeijer-Hazeleger et al. [20] reported that the type of carrier gas effects the rate of adsorption and the shape of the adsorption isotherm in zeolites. They found that this is more pronounced at lower pressures and temperatures.

In this study, the K_{eq_i} and ΔH are estimated in the absence of carrier gas, in vacuum and at conditions of very low coverage by a transient method. One should recall that the equilibrium constant defined as $K_{eq_i} = q_{\max_i} \frac{k_{a_i}}{k_{d_i}}$ is the product of the maximum sites available for the adsorption of species *i* and the ratio of the adsorption and desorption rate constants for species *i*. In TAP experiments only the ratios of characteristic desorption and adsorption times are obtained but no independent information is available on $q_{\max_i}$ which logically speaking represents the maximum sites available at zero coverage. In other techniques as mentioned above the equilibrium constant values are obtained directly by the ratio of the adsorbed to bulk normalized concentrations. Thus any changes in $q_{\max_i}$ with species, or from zeolite to zeolite, are reflected through the values of normalized adsorbed equilibrium concentrations. In the TAP case, one relies on the established fact that equilibrium properties like K_{eq_i} can be assessed by a dynamic experiment as long as the system is linear. However, that assumes perfect measurement as often the information is buried in the tail of the response curve which is not readily measured. In the TAP experiment we cannot capture the equilibrium values directly but we can obtain the ratios of the characteristic times for adsorption and desorption and from them evaluate the equilibrium constant. The problem in obtaining accurate values lies in the fact that the accessible $q_{\max_i}$ varies with temperature and this is reflected in the characteristic adsorption time. One would expect that as molecular mobility increases with temperature more active sites can be reached at higher temperature. Thus the apparent $q_{\max_i}$, which is sensed experimentally via TAP response through the adsorption desorption time constants, becomes larger. While the ratio of the adsorption and desorption constants decreases with temperature, the rise in $q_{\max_i}$ with temperature reduces the apparent heat of adsorption. It should be noted that while the absolute values of the heats of adsorption are much lower as determined by TAP, the trends on the same zeolite for two species are the same as determined by other techniques. The difference between zeolites for the same species also tracks the trend established by equilibration techniques. For example, the apparent heat of adsorption values estimated in this study for isobutane in beta and USY zeolites are 23.6 (s.d. 2.32) kJ/mole and 14.6 (s.d. 1.85) kJ/mole, respectively, in comparison to the heat of adsorption values for isobutane in beta and USY zeolites as 47 ± 4 kJ/mole and 35 ± 4 kJ/mole, respectively, as reported in the literature [17]. This confirms that in transient techniques such as, TAP there is not sufficient time for equilibration of gas and solid phase. As a result, the

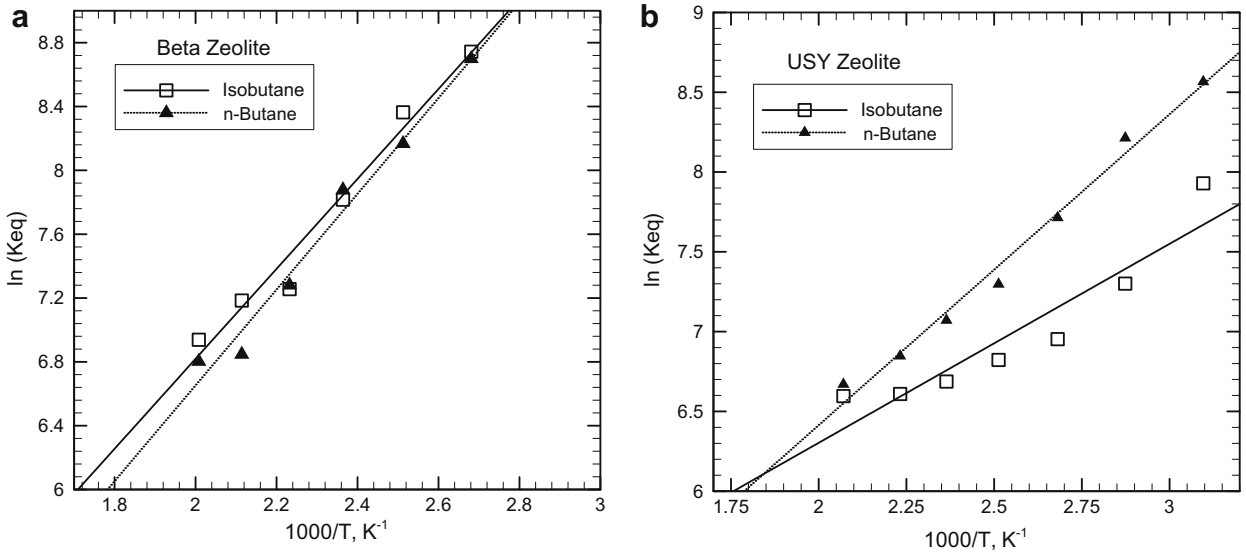

Fig. 10. van't Hoff plot for equilibrium constant K_{eq_i} calculated for isobutane and *n*-butane in beta (a) and USY (b) zeolites using single pulse TAP response experiments.

molecules do not reach all the adsorption sites of high energy [51], hence, further decreasing the apparent heat of adsorption. This is why we call this quantity apparent heat of adsorption.

It should also be mentioned that as the temperature increases the octahedral coordinated aluminum (Al) is converted to tetrahedral coordination [52,53] and the tetrahedral coordinated Al species are Brønsted sites [52,53]. It has been reported that at low surface coverage the adsorption occurs only on the Brønsted acid sites in zeolites [15,16]. As a result, the maximum concentration of adsorption sites will increase with temperature making more sites available during the TAP experiment. If one represented the increase in accessible sites with temperature with an Arrhenius type dependence that would explain the reduction in the observed heat of adsorption while maintaining the van't Hoff's plot linearity.

It is noteworthy that semi-quantitatively the apparent heats of adsorption for isobutane and *n*-butane in USY and beta zeolites obtained from TAP experiments match the trends reported in the literature. In USY zeolite the apparent heat of adsorption for *n*-butane is higher than for isobutane which is in agreement with the values observed by other researchers such as Gong and Denayer et al. [16,17]. The weak adsorption of isobutane in USY zeolite is likely due to its ramified skeleton which allows easier motion of adsorbed molecules from site to site in USY zeolite [16]. In beta zeolite the apparent heat of adsorption for isobutane is slightly lower than for *n*-butane (see Table 4). This is in agreement with the heat of adsorption values reported in the literature for alkanes in beta zeolite [16].

It is also observed that the apparent heat of adsorption for either of the two tested species in beta zeolite is higher than in USY zeolite (see Table 4). This is in comparison with the literature as shown above. As mentioned earlier, the beta zeolite framework consists of straight and zig-zag 12-membered-ring channels of maximum free aperture 0.71 nm compared to USY zeolite framework, which contains a super cage of free aperture 1.2 nm. As a result, the distance between the adsorbed molecules and beta zeolite framework is shorter than in USY, causing a stronger dispersive interaction and thus a higher heat of adsorption in beta zeolite.

5.6. Intra-particle diffusion time $\left(D_{e_i}/R_p^2\right)^{-1}$

As mentioned earlier, only the dimensionless parameter $\tau_{p_i}\left(\tau_{p_i}=\frac{L^2/D_{K_i}}{R_p^2/D_{e_i}}\right)$ estimated for isobutane and *n*-butane pulsed over beta zeolite falls inside the model sensitivity range shown in Table 2. Hence, only these τ_{p_i} values with their standard deviation and 95% confidence interval at various temperatures, are shown in Table 5. The characteristic time for intra-particle diffusion $\left(R_p^2/D_{e_i}\right)$ is then estimated at each temperature by multiplying the τ_{p_i} obtained for the model match of experimental results by the characteristic diffusion time in the micro-reactor $\left(L^2/D_{K_i}\right)$. An Arrhenius plot of the intra-particle diffusivities (reciprocal values of intra-particle diffusion times) is shown in Fig. 11 and the activation energies (E_a) and pre-exponential factors $\left(D_{e_i}^0/R_p^2\right)$ obtained from the Arrhenius plot are also presented in Table 5. It is observed that the intra-particle diffusivities of *n*-butane and isobutane have the same order of magnitude and similar activation energies. These similarities indicate that the large micro-pore beta zeolite (pore diameter ~0.69 nm) is not very shape selective for small molecules of similar diameter (kinetic diameter of isobutane ~0.58 nm and of *n*-butane ~0.52 nm).

Table 5
The values of the dimensionless parameter τ_{p_i}, with the standard deviation and 95% confidence interval, and activation energies (E_a) and pre-exponential factors $\left(D_{e_i}^0/R_p^2\right)$ obtained from the Arrhenius plot, estimated over a thin zone of beta zeolites.

Probe molecules	T (K)	τ_{p_i} ($\times10^{-5}$)	Std. deviation ($\times10^{-6}$)	95% Confidence interval ($\times10^{-5}$)	E_a (kJ/mole)	$\left(D_{e_i}^0/R_p^2\right)$ s^{-1}
Isobutane	373	1.240	1.21	1.120 to 1.360	20.9	0.026
	398	1.850	0.65	1.780 to 1.920	(s.d.	(s.d. 1.8 e^{-3})
	423	1.810	0.78	1.730 to 1.890	2.78)	
	448	2.330	4.05	1.930 to 2.740		
	473	3.900	4.89	3.500 to 4.310		
	498	4.710	4.70	4.310 to 5.120		
Butane	373	1.290	0.51	1.240 to 1.340	20.5	0.024
	398	1.500	0.59	1.440 to 1.560	(s.d.	(s.d. 1.7 e^{-3})
	423	1.700	2.88	1.410 to 1.990	3.08)	
	448	2.340	4.67	1.870 to 2.810		
	473	3.920	4.70	3.450 to 4.390		
	498	4.270	4.08	3.800 to 4.700		

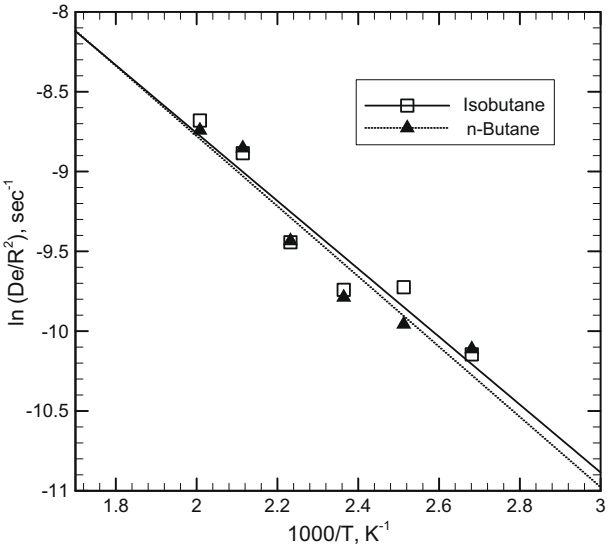

Fig. 11. Arrhenius plot for characteristic time for intra-particle diffusion $\left(D_{e_i}/R_p^2\right)$ calculated for isobutane and *n*-butane in beta zeolite using single pulse TAP response experiments.

Based on the activation energies and pre-exponential factors reported in Table 5, the intra-particle diffusivities are estimated as 1.4×10^{-10} m^2/s for isobutane/beta zeolite and 1.1×10^{-10} m^2/s for butane/beta zeolite with particle size of 5 μm at 373 K. This intra-particle diffusivity values are in agreement with the range of the intra-particle diffusivities values reported in the literature for large pore zeolites [25]. In comparison to this study the values of intra-particle diffusivity in zeolites of a similar pore aperture obtained by the other macroscopic experimental systems [25] are one or two order of magnitude lower. For example, Karger and Ruthven [25] reported the diffusivity value for *n*-butane in Na-X zeolite as 4.9×10^{-11} m^2/s for crystal size of 50 μm at 423 K. The lower estimates are attributed to additional extra-crystalline mass transfer resistance and the presence of carrier gas in the macroscopic experimental systems [25,35]. The diffusivity values obtained for isobutane and *n*-butane in beta zeolite using the crystallites average size of 0.3 μm are 4.9×10^{-13} m^2/s and 4.1×10^{-13} m^2/s, respectively, at 373 K.

6. Conclusions

The thin zone TAP micro-reactor experiments are used to observe adsorption–desorption dynamics for *n*-butane and isobutane and to evaluate their pertinent parameters in beta and USY zeolites. It is established that various system parameters can only be

reliably estimated from a single pulse TAP experiment in a thin zone micro-reactor when the three dimensionless constants of the model fall into certain ranges. Since these constants are not known 'a priori', reliable estimation of system parameters may involve an iterative procedure of experimental design and data interpretation to establish the range of constants needed for reliable estimates. For isobutane and *n*-butane the values of the apparent heat of adsorption (ΔH), intra-particle diffusivity $\left(D_{e_i}^0/R_p^2\right)$ and its activation energy (E_a) in beta zeolite have been presented, as the sensitivity criteria were met. Only the apparent heat of adsorption (ΔH) in USY zeolites can be estimated from the performed experiments. The intra-particle diffusivity estimated by the TAP response experiments is obtained at very low surface coverage, and these data can provide a test for various theories such as molecular dynamics, transition-state theory, mean-field theories and Monte-Carlo techniques. The thin zone reactor configuration enabled the use of small beta and USY zeolite particles without high bed resistance.

The apparent heat of adsorption in beta zeolite is higher than in USY zeolite, due to shorter distance between adsorbed molecules in the beta zeolite frame work. Based on the values of the apparent heat of adsorption and the intra-particle diffusivity it is concluded that the branching of the C4 alkanes has little effect in beta zeolites. However, the USY zeolite preferentially adsorbs *n*-butane compared to isobutane. Based on the parameters estimated for isobutane and *n*-butane in USY, which are outside the permissible model sensitivity range, it is concluded that intra-particle diffusivity and desorption constant cannot be reliably estimated from the conducted TAP experiments. A redesign of experimental conditions is required to bring the parameters into the acceptable sensitivity range. Specifically, to obtain the reliable estimates of these parameters, the experiments should be carried out with larger inert particles or with a shorter micro-reactor length.

It is noted that while the trends in the apparent heats of adsorption obtained from the TAP experiments (e.g. variation from species to species on the same zeolite, or variation of a value for a given species from zeolite to zeolite) are in agreement with the values reported in the literature, the TAP determined apparent heats of adsorption are considerably lower in absolute value. It was concluded that this most likely is due to the variation with temperature of the maximum active sites accessible to the probe molecules. Thus, without additional calibration for total sites available at zero coverage as function of temperature the TAP experiment cannot be expected to produce quantitative measures of the traditional heat of adsorption as obtainable by other techniques that require equilibration of the sample. However, TAP offers opportunities for quantification of dynamics of transport and adsorption–desorption in the particles if the experimental design is carefully chosen.

Acknowledgments

The authors thank Dr. John Gleaves from Washington University in St. Louis for making the TAP instrument available for this research. They also thank the National Science Foundation (Grant EEC-0310689) and the Center for Environmentally Beneficial Catalysis (CEBC) for financial support.

References

[1] M.C. Clark, B. Subramaniam, Ind. Eng. Chem. Res. 37 (1998) 1243–1250.
[2] K.P. de Jong, C.M.A.M. Mesters, D.G.R. Peferoen, P.T.M. van Brugge, C. de Groot, Chem. Eng. Sci. 51 (1996) 2053–2060.
[3] A. Feller, J.A. Lercher, Adv. Catal. 48 (2004) 229–295.
[4] M.F. Simpson, J. Wei, S. Sundaresan, Ind. Eng. Chem. Res. 35 (1996) 3861–3873.
[5] A. Gianetto, H.I. Farag, A.P. Blasetti, H.I. de Lasa, Ind. Eng. Chem. Res. 33 (1994) 3053–3062.
[6] I. Pitault, D. Nevicato, M. Forissier, J.-R. Bernard, Chem. Eng. Sci. 49 (1994) 4249–4262.
[7] V.W. Weekman, D.M. Nace, AIChE J. 16 (1970) 397–404.
[8] S. Gopal, P.G. Smirniotis, J. Catal. 225 (2004) 278–287.
[9] S. Phatanasri, P. Praserthdam, S. Kularbkeaw, S. Panichsarn, React. Kinet. Catal. Lett. 71 (2000) 281–287.
[10] R. Roldán, F.J. Romero, C. Jiménez-Sanchidrián, J.M. Marinas, J.P. Gómez, Appl. Catal. A 288 (2005) 104–115.
[11] Z.B. Wang, A. Kamo, T. Yoneda, T. Komatsu, T. Yashima, Appl. Catal. A 159 (1997) 119–132.
[12] B.G. Anderson, F.J.M.M. de Gauw, N.J. Noordhoek, L.J. van Ijzendoorn, R.A. van Santen, M.J.A. de Voigt, Ind. Eng. Chem. Res. 37 (1998) 815–824.
[13] P.S. Bárcia, J.A.C. Silva, A.E. Rodrigues, Micropor. Mesopor. Mater. 79 (2005) 145–163.
[14] P.S. Bárcia, J.A.C. Silva, A.E. Rodrigues, Stud. Surf. Sci. Catal. 170 (1) (2007) 955–960.
[15] J.F. Denayer, G.V. Baron, J.A. Martens, P.A. Jacobs, J. Phys. Chem. B 102 (1998) 3077–3081.
[16] J.F. Denayer, W. Souverijns, P.A. Jacobs, J.A. Martens, G.V. Baron, J. Phys. Chem. B 102 (1998) 4588–4597.
[17] K. Gong, Adsorption/desorption Studies on Solid Acid Alkylation Catalysts Using a Tapered Element Oscillating Microbalance (TEOM), University of Kansas, 2008.
[18] C.K. Lee, S. Ashtekar, L.F. Gladden, P.J. Barrie, Chem. Eng. Sci. 59 (2004) 1131–1138.
[19] P.M. Lima, C.V. Gonçalves, C.L. Cavalcante Jr, D. Cardoso, Micropor. Mesopor. Mater. 116 (2008) 352–357.
[20] M.C. Mittelmeijer-Hazeleger, A.F.P. Ferreira, A. Bliek, Langmuir 18 (2002) 9613–9616.
[21] Y. Schuurman, C. Delattre, I. Pitault, J.P. Reymond, M. Forissier, Chem. Eng. Sci. 60 (2005) 1007–1017.
[22] M.J. Truitt, J.L. White, Solid State Nucl. Magn. Reson. 35 (2009) 100–103.
[23] A. Wender, A. Barreau, C. Lefebvre, A. Di Lella, A. Boutin, P. Ungerer, A. Fuchs, Adsorption 13 (2007) 439–451.
[24] J. Zhang, Z. Zhao, A. Duan, G. Jiang, J. Liu, D. Zhang, Energy Fuels 23 (2009) 617–623.
[25] J. Karger, D.M. Ruthven, Diffusion in Zeolites and Other Microporous Solids, John Wiley and Sons, New York, 1992.
[26] V. Iyengar, M.-O. Coppens, Chem. Eng. Sci. 59 (2004) 4747–4753.
[27] D.F. Plant, G. Maurin, I. Deroche, L. Gaberova, P.L. Llewellyn, Chem. Phys. Lett. 426 (2006) 387–392.
[28] A.I. Skoulidas, D.S. Sholl, J. Phys. Chem. A 107 (2003) 10132–10141.
[29] M. Eic, D.M. Ruthven, Zeolites 8 (1988) 40–45.
[30] M. Hagelstein, U. Hatje, H. Förster, T. Ressler, W. Metz, Stud. Surf. Sci. Catal. 84 (2) (1994) 1217–1222.
[31] H.G. Karge, W. Nießen, Catal. Today 8 (1991) 451–465.
[32] N.S. Raghavan, D.M. Ruthven, AIChE J. 29 (1983) 922–925.
[33] N.S. Raghavan, D.M. Ruthven, Chem. Eng. Sci. 40 (1985) 699–706.
[34] O.P. Keipert, M. Baerns, Chem. Eng. Sci. 53 (1998) 3623–3634.
[35] T.A. Nijhuis, L.J.P. van den Broeke, M.J.G. Linders, J.M. van de Graaf, F. Kapteijn, M. Makkee, J.A. Moulijn, Chem. Eng. Sci. 54 (1999) 4423–4436.
[36] J.T. Gleaves, G.S. Yablonskii, P. Phanawadee, Y. Schuurman, Appl. Catal. A 160 (1997) 55–88.
[37] S.O. Shekhtman, G.S. Yablonsky, J.T. Gleaves, R. Fushimi, Chem. Eng. Sci. 58 (2003) 4843–4859.
[38] J.A. Delgado, T.A. Nijhuis, F. Kapteijn, J.A. Moulijn, Chem. Eng. Sci. 59 (2004) 2477–2487.
[39] B. Zou, M.P. Dudukovic, P.L. Mills, Chem. Eng. Sci. 48 (1993) 2345–2355.
[40] C. Baerlocher, W.M. Meier, D.H. Olson, Atlas of Zeolite Framework Types, Elsevier, Amsterdam, 2001.
[41] J.M. Smith, Chemical Engineering Kinetics, McGraw-Hill, New York, 1981.
[42] L.J.P. Van Den Broeke, R. Krishna, Chem. Eng. Sci. 50 (1995) 2507–2522.
[43] R. Krishna, R. Baur, Sep. Purif. Technol. 33 (2003) 213–254.
[44] D. Paschek, R. Krishna, Chem. Phys. Lett. 333 (2001) 278–284.
[45] R.J. Berger, F. Kapteijn, J.A. Moulijn, G.B. Marin, J. De Wilde, M. Olea, D. Chen, A. Holmen, L. Lietti, E. Tronconi, Y. Schuurman, Appl. Catal. A 342 (2008) 3–28.
[46] R. Feres, G. Yablonsky, Chem. Eng. Sci. 59 (2004) 1541–1556.
[47] M. Olea, Y. Iwasawa, Appl. Catal. A 275 (2004) 35–42.
[48] W.E. Schiesser, C.A. Silebi, Computational Transport Phenomena: Numerical Methods for the Solution of Transport Problems, Cambridge University Press, Cambridge, UK, 1997.
[49] P.T. Boggs, R.H. Byrd, R.B. Schnabel, SIAM J. Sci. Stat. Comput. 8 (1987) 1052–1078.
[50] D.M. Ruthven, L.-K. Lee, AIChE J. 27 (1981) 654–663.
[51] J.L. Condor, C.L. Young, Physicochemical Measurements by Gas-Adsorption Chromography, John Wiley and Sons, Chicester, UK, 1979.
[52] A. Omegna, R. Prins, J.A. van Bokhoven, J. Phys. Chem. B 109 (2005) 9280–9283.
[53] W. Zhang, P.G. Smirniotis, M. Gangoda, R.N. Bose, J. Phys. Chem. B 104 (2000) 4122–4129.